ADVANCED FUNCTIONAL MATERIALS
www.afm-journal.de

Structural Color Liquids with Sol-Gel Irreversibility for Visualized Freeze-Thaw Monitoring

*Qilong Zhao, Chao Huang, and Xuemin Du**

Protein-based bio-products such as vaccines, antibodies, enzymes, and plasma are crucial in public health and life sciences, yet their efficacy is frequently compromised by temperature fluctuations, especially repeated freeze-thaw cycles during storage and transport. While monitoring freeze-thaw damage is critical for the quality control of these bio-products, current methods lack the capability to indicate the exact number of freeze-thaw cycles. Here, structural color liquids enable visualized freeze-thaw monitoring (FT-SCLs) are introduced by harnessing their irreversible sol-gel phase transition under repeated freeze-thaw cycles, which are constructed by assembling periodically structured poly(styrene-acrylic acid) colloidal particles within a poly(vinyl alcohol) suspension. The FT-SCLs undergo irreversible sol-gel transition and therefore unidirectional alteration of their periodic structures during freeze-thaw cycling, imparting stepwise and unrecoverable color change (from red to green) to indicate the exact number of freeze-thaw cycles. Through modulating the sol-gel transition, the FT-SCLs are constructed with adjustable sensitivity across practically relevant temperature ranges (−80–−4 °C) and customizable response thresholds for diverse application scenarios. Leveraging their unique capabilities of freeze-thaw monitoring via non-tampered optical signals, such FT-SCLs exhibit broad applicability in vaccine storage, whole blood preservation, and enzyme stability monitoring, which can further be extended for cell cryopreservation and the food industry.

1. Introduction

Protein-based bio-products such as vaccines, antibodies, enzymes, and plasma play vital roles in public healthcare and life sciences, where the annual market sales of vaccines alone are more than 19 billion dollars.[1] To ensure their potency, these bio-products are required to be stored or distributed via cold chain (0–8 °C, or below −18 °C) due to their temperature susceptibility.[2] Unfortunately, temperature excursions are frequently encountered in the cold chain, which affects over half of vaccines.[3] Among them, inadvertent freezing, especially freeze-thaw cycling, contributes to 75–100% of temperature-related accidents.[4] However, monitoring the damage induced by freeze or freeze-thaw cycling remains a great challenge. It currently relies on electronic loggers for recording the life-cycle temperature history and shake tests for examining the potency;[5] whereas many limitations still exist. First, such methods need professional operators and complicated equipment, hindering their broad applications. Second, the uses of electronic loggers bring problems of high cost, environmental harm caused by electronic waste, and the risk of data manipulation. Third, the shake tests can only distinguish between freeze-damaged and non-freezing samples but cannot indicate the exact number of freeze-thaw cycles. Considering the freeze-thaw cycle number is a key factor correlated with the potency of bio-products as the protein conformation is affected with increased cycles,[6] it will be urgent to develop methods to monitor the exact number of freeze-thaw cycles in facile and intuitive manners for these temperature susceptible bio-products.[7]

Over the past decades, intelligent labels that can monitor the temperature history via intuitive coloration have emerged,[8] which show many merits such as easy handling, direct readability, and low cost.[9] To date, commercially available products, including Berlinger VCCM-Card and 3M Freeze Watch Indicators, have been developed for visualized monitoring of freeze damage. But those labels can solely alert freeze damage for one time as their color can solely be changed once when the freeze-induced fracture of dye-filled ampules. Even worse, these labels encounter problems of unreliability caused by photobleaching, degradation, and/or leakage of chemical dyes.[10] Alternatively, structural color materials that possess periodic structures to interact with light waves have opened new avenues of intelligent labels, whose colors are highly stable and independent of chemical dyes.[11] By introducing stimuli-responsive components, smart structural color materials can further alter their colors through changing their periodic structures in response to specific external stimuli,[12] making them promising colorimetric sensors for monitoring a variety of signals, ranging from force,[13] electric,[14]

Q. Zhao, C. Huang, X. Du
Center for Intelligent Biomedical Materials and Devices (IBMD)
Shenzhen Institutes of Advanced Technology (SIAT)
Chinese Academy of Sciences (CAS)
Shenzhen 518055, P. R. China
E-mail: xm.du@siat.ac.cn
X. Du
Key Laboratory of Biomedical Imaging Science and System
Chinese Academy of Sciences
Shenzhen 518055, P. R. China

The ORCID identification number(s) for the author(s) of this article can be found under https://doi.org/10.1002/adfm.202500381

DOI: 10.1002/adfm.202500381

magnetic,[15] chemicals,[16] to heat.[17] As a new class of smart structural color materials, emerging structural color liquids with metastable structures and particular superiorities in sensitivity have attracted increasing attention.[18] Based on these highly sensitive structural color liquids, our studies have recently reported intelligent labels enabling inspection of risky heat exposure,[19] whose colors are changed during temperature rise as their periodic structures are irreversibly deconstructed under one-time phase transition from freezing to melting states through the introduced triggering agents. Nevertheless, how the alternate phase transition during freeze-thaw cycling affects the periodic structures of structural color liquids remains unclear, thus lacking corresponding techniques enabling freeze-thaw monitoring via intuitive coloration.

Here, we introduce structural color liquids for visualized freeze-thaw monitoring (FT-SCLs) by harnessing their irreversible sol-gel phase transition under freeze-thaw cycling (**Figure** 1A,B). The FT-SCLs consist of orderly assembled poly(styrene-acrylic acid) (PS) colloidal particles within PVA suspensions. Despite fluidic status, the FT-SCLs can preserve their stable structural color at common cold-chain temperatures (0 °C, 8 °C, or −20 °C). Upon exposure to repeated freeze-thaw cycles, the FT-SCLs exhibit irreversible sol-gel transition and thereby unidirectional alteration of their periodic structures, imparting stepwise and unrecoverable color change (from red to green) to indicate the exact number of freeze-thaw cycles. Through modulating the sol-gel transition, the FT-SCLs further demonstrate adjustable sensitivity across practically relevant temperature ranges (−80–−4 °C) and customizable response thresholds for diverse application domains. Leveraging on the unprecedented capability of visualized freeze-thaw monitoring, the FT-SCLs provide intuitive signs to warn of the loss of potency for diverse bio-products such as vaccines, whole blood, and horseradish peroxidase enzymes (HRP) under multiple freeze-thaw cycles. Beyond the quality control of temperature-sensitive bio-products in the cold chain, the FT-SCLs also have broad implications in cell cryopreservation and the food industry.[20]

2. Results and Discussion

2.1. Fabrication of FT-SCLs

The FT-SCLs are constructed by assembling PS particles within rationally formulated PVA suspensions (Figure S1, Supporting Information). Mono-dispersed PS particles are synthesized according to the established soap-free emulsion polymerization method.[21] The synergic inter-particle interactions, including van der Waals attraction and electrostatic repulsion, drive their spontaneous assembly at supersaturated conditions.[22] Meanwhile, the suspension is prepared by mixing a PVA solution (10.0 wt% PVA in a dimethyl sulfoxide (DMSO)/water (50/50/w) mixture solvent), glycerol, and carbon black powders in a mass ratio of 90:9.8:0.2, which is rationally formulated for the following three reasons. First, the PVA solution poses a unique feature of irreversible sol-gel transition under freeze-thaw cycling.[23] Second, the presence of glycerol and DMSO can stabilize the assembly and prevent the aggregation of the colloidal particles by increasing the viscosity.[18b] Third, the addition of carbon black powders can enhance the color contrast by reducing light scattering.[34] Owing to the rationally designed formulation, PS colloidal particles are orderly assembled into periodically structured microcrystals within the suspension at the specific mass ratio (50 wt%, Figure 1C), endowing the FT-SCLs with vivid structural colors.[12a] Notably, the FT-SCLs exhibit a fluidic state, which preserves the capability of sol-gel transition, distinctly different from existing PVA-based structural color materials with dried PVA matrix or cross-linked PVA networks.[24] The color of FT-SCLs is sensitive to the variations of the mass ratio of the colloidal particles within the suspensions. Low mass ratios of PS particles (30 or 40 wt%) lead to colorless or unbright colors owing to non-saturation and large inter-particle distance, while increasing the mass ratios of PS particles to 60 wt% still induces a decrease in relative intensity as the ordered periodic structures are hard to form within the assembly period of 24 h (Figure 1D). Additionally, the original colors of the FT-SCLs can be facilely tuned into blue, green, or red by using the PS colloidal particles with different average diameters (181, 192, or 225 nm, Figure 1E; Figure S2, Supporting Information). Moreover, the FT-SCLs can be facilely processed into as-wanted patterns such as QR codes and labels (Figure S3, Supporting Information), showing versatility for practical applications.

Despite fluidic states,[18b,c] the FT-SCLs still exhibit highly stable structural color owing to the high viscosity that can stabilize the assembled colloidal particles by inhibiting Brownian motion.[19] Even when exerting an external force, they can rapidly recover to their original color once the force was withdrawn (Movie S1, Supporting Information). Additionally, the structural color of the FT-SCLs also preserves high stability in the common conditions of the cold chain (0, 8, or −20 °C) over time as the sol-gel transition would not occur without freeze-thaw cycling (Figure 1F). In either thawing (0–8 °C) or freezing (−20 °C) states, the FT-SCLs show non-changed color over dozens of days, whose reflection shifts less than 10 nm (Figure 1G; Figure S4, Supporting Information). These results reveal that the FT-SCLs can avoid incorrect alarms during cold-chain storage or transport.

2.2. Irreversible Color Change Within Multiple Freeze-Thaw Cycles

We next examine whether the FT-SCLs can monitor freeze-thaw cycling via color changes (**Figure** 2A). After the 1st freeze-thaw cycle (freezing at −20 °C and thawing at 8 °C), the FT-SCLs slightly change their original red color to orange color, with a blueshift in the reflection of 13 nm (Figure 2B). After the following 2nd and 3rd freeze-thaw cycles, the color of FT-SCLs turns yellow and ultimately green, whose changes can be recognized by the naked eye, with a maximum blueshift of 30 nm in the reflection (Figure 2B). Notably, the color change of the FT-SCLs is irreversible during the alternate phase transition within multiple freeze-thaw cycles, which cannot be realized by existing thermos-responsive structural color materials based on the thermo-responsive hydrogels that exhibit reversible color changes during the alternate phase transition.[12b,c] Moreover, the changed color of the FT-SCLs after multiple freeze-thaw cycles cannot be recovered at either cryogenic condition (−30 °C) or room temperature (25 °C, Figure S5, Supporting Information), indicating that they can provide

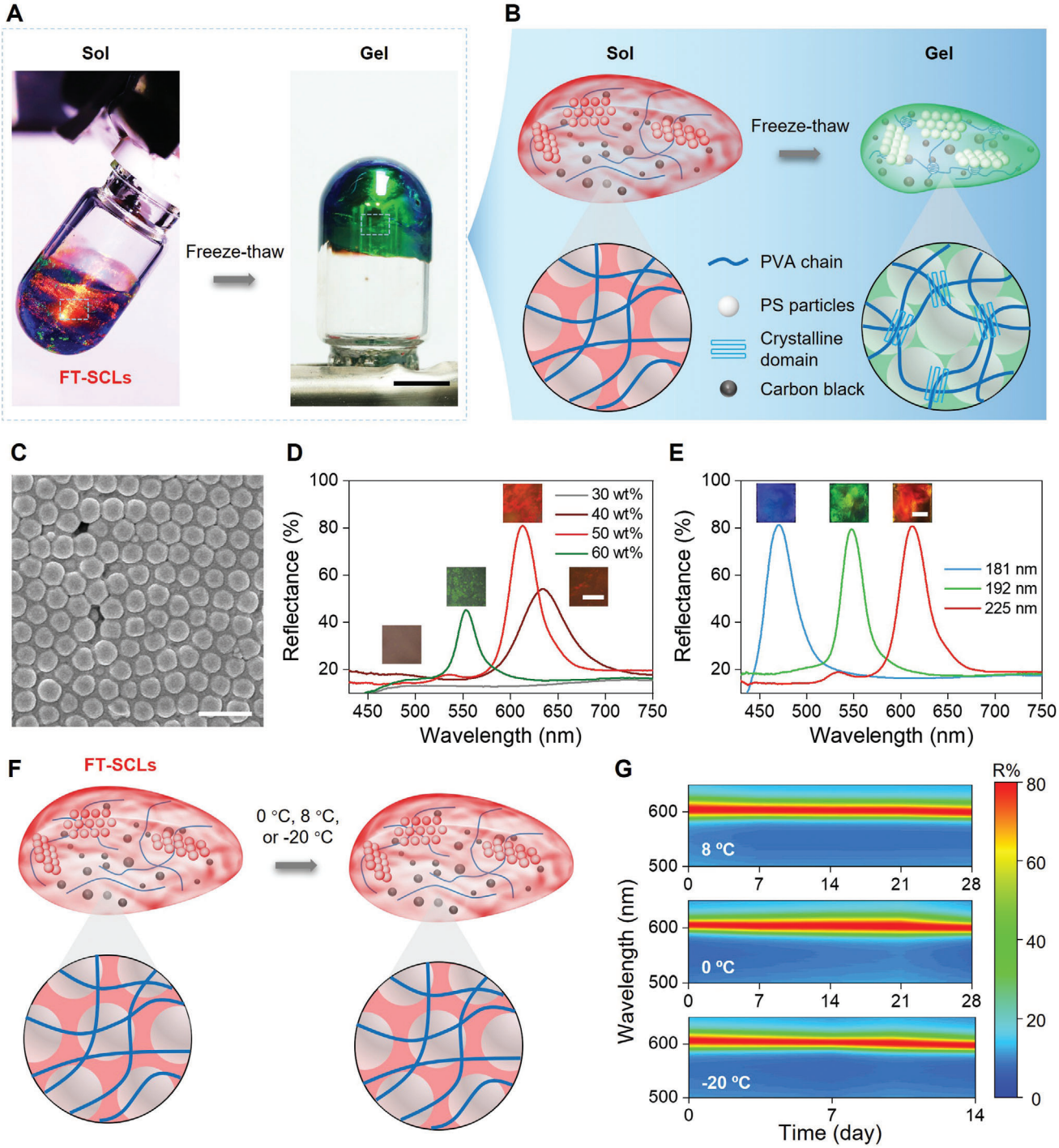

Figure 1. Fabrication of FT-SCLs. A) Representative macroscopic images of the FT-SCLs before and after multiple freeze-thaw cycles, showing irreversible color changes along with an irreversible sol-gel transition. Scale bar: 5 mm. B) Schematic illustrating the changes in color and periodic structures of the FT-SCLs under repeated freeze-thaw cycles. The FT-SCLs undergo an irreversible sol-gel transition that leads to unidirectional alteration of their periodic structures, thus imparting stepwise and unrecoverable color change. C) Representative scanning electronic microscopic (SEM) image of the FT-SCLs. Scale bar: 500 nm. D) Macroscopic images and reflection spectra of the FT-SCLs formed at diverse mass ratios of PS colloidal particles (30–60 wt%). Scale bar: 1 cm. E) Macroscopic images and reflection spectra of FT-SCLs formed by using the PS colloidal particles with different diameters (181 for blue, 192 for green, and 225 nm for red). Scale bar: 1 cm. F) The FT-SCLs maintain their original color when kept in common conditions of cold-chain storage (0, 8, or −20 °C) as their periodic structures do not change. G) Dynamic reflectance contour spectra of FT-SCLs at 8, 0, or −20 °C over time. Scale bars: 200 μm.

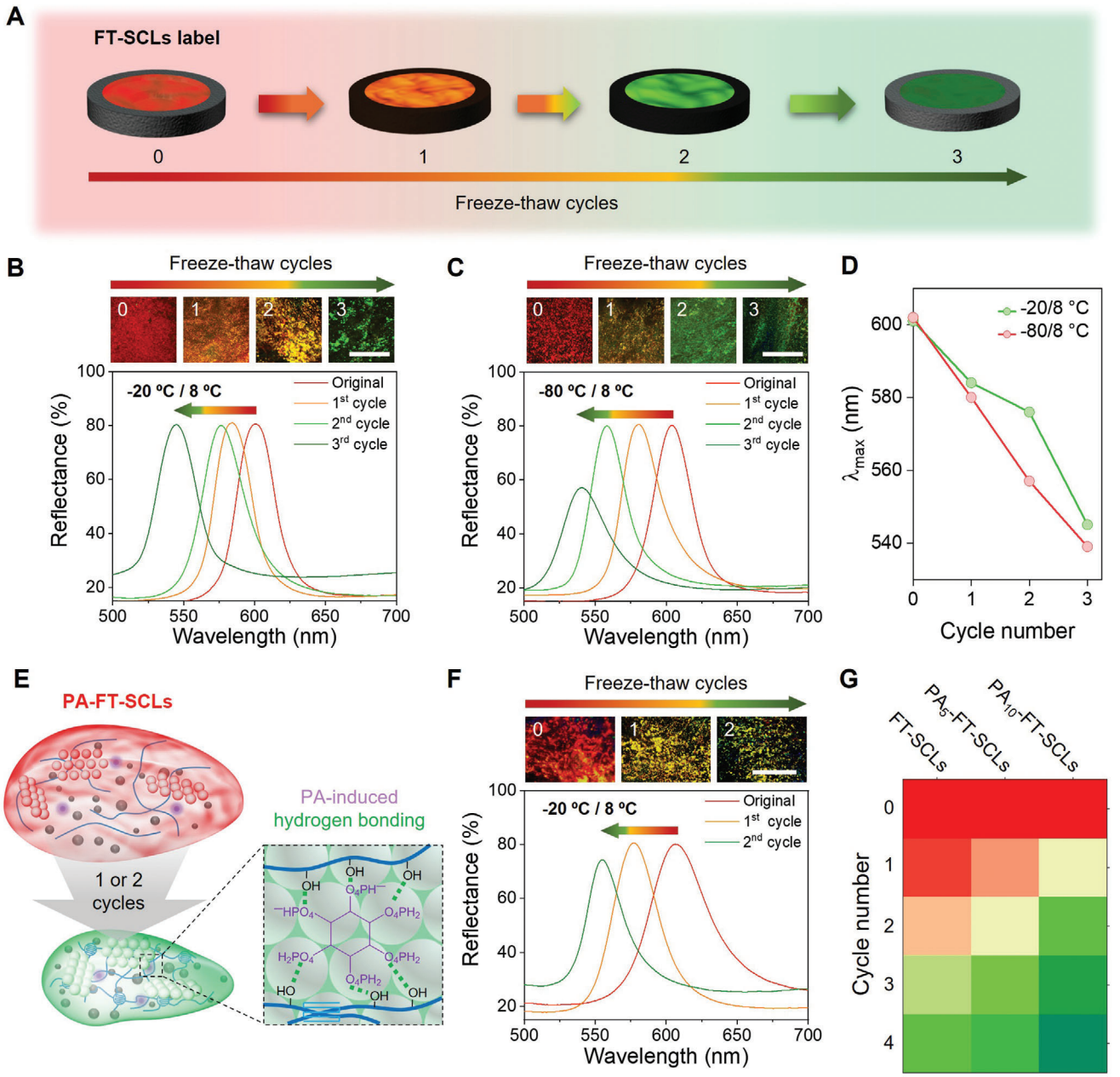

Figure 2. Irreversible color change within multiple freeze-thaw cycles. A) Schematic diagram of FT-SCLs with altered colors for freeze-thaw monitoring. B,C) Microscopic images and reflectance spectra of FT-SCLs labels under multiple freeze-thaw cycles with the thawing temperature of 8 °C and different freezing temperatures of −20 °C (B) or −80 °C (C). Scale bars: 500 μm. D) Statistics of the shift of reflection peaks (λ_{max}) over diverse freeze-thaw cycles with the thawing temperature of 8 °C and different freezing temperatures of −20 °C or −80 °C. E,F) Schematic diagram (E), microscopic images, and reflectance spectra (F) of PA-introduced FT-SCLs under multiple freeze-thaw cycles with a freezing temperature of −20 °C and a thawing temperature of 8 °C. Scale bars: 500 μm. G) The colorimetric map of the FT-SCLs with PA-free formulation (FT-SCLs), PA contents of 5 wt% (termed "PA_5-FT-SCLs"), or 10 wt% (termed "PA_{10}-FT-SCLs") to indicate specific numbers of freeze-thaw cycles with the freezing temperature of −20 °C and thawing temperature of 8 °C.

non-tampered optical signals to reliably record the freeze-thaw history. Additionally, the FT-SCLs are also applicable to monitor the freeze-thaw processes with a freezing temperature down to −80 °C. Under repeated freeze-thaw cycles with respective freezing and thawing temperatures of −80 and 8 °C, the FT-SCLs still demonstrate an irreversible color change from red to olive green, with an accelerated shift in the refection over multiple freeze-thaw cycles (Figure 2C,D), inferring that they can be used for the bio-products that require to be stored at super-cold conditions, e.g., mRNA vaccines.[25]

We then investigate how to tune the responsiveness of the FT-SCLs in freeze-thaw monitoring via modulating their

sol-gel transition. PVA with decreased alcoholysis degrees presents increased amounts of carboxyl groups, which impede the formation of ice crystals for the solvents (i.e., DMSO-hydrates).[26] Therefore, the FT-SCLs formulated by using the PVA with a decreased alcoholysis degree (from 88% to 80%) exhibit a declined triggered temperature (T_{tigger}: −28 °C, Figure S6A, Supporting Information). Such FT-SCLs can maintain their original red color after 3 freeze-thaw cycles with the freezing temperature of −20 °C (Figure S6B, Supporting Information) yet demonstrate apparent color change (from red to green) and significant refection shift ($\Delta\lambda > 60$ nm) within the freeze-thaw cycles with a lower freezing temperature of −30 °C (Figure S5C, Supporting Information). The FT-SCLs with a low $T_{trigger}$ will be applicable to some enzymes,[27] which are normally stored at −20 °C but lose their potency at a lower temperature. In addition to the $T_{trigger}$, the sensitivity and response thresholds of the FT-SCLs can also be adjusted by tuning the sol-gel transition. The sol-gel transition of the FT-SCLs can be accelerated by introducing phytic acid (PA), which can generate intermolecular hydrogen bonding with PVA (Figure 2E).[28] Accordingly, such PA-introduced FT-SCLs behave with superior sensitivity to freeze-thaw cycles and faster color-change rates than PA-free samples, as represented by obvious color changes (from green to yellow) and significant shifts of reflection peak ($\Delta\lambda > 20$ nm) after 2 and even only 1 cycle (Figure 2F; Figure S7, Supporting Information). Interestingly, the $T_{trigger}$ of the PA-introduced FT-SCLs can be up to −4 °C, near the critical temperature, when the introduced PA contents reach 10 w w%$^{-1}$ (Figure S8, Supporting Information). Their $T_{trigger}$ will be estimated to be further modulated by adding higher contents of PA. Overall, through modulating the sol-gel transition, we can formulate the FT-SCLs with adjustable sensitivity and response thresholds to monitor the freeze-thaw processes with diverse $T_{trigger}$ (−80–−4 °C) and tuneable cycle numbers for specific application scenarios (Figure 2G; Figure S9, Supporting Information), which can be used for not only vaccines requiring highly sensitive color alteration within one freeze-thaw cycle but also the identification of enzyme bioactivity loss by recording multiple cycles.[1,6]

2.3. Freeze-Thaw Monitoring Mechanisms

We next study the mechanisms underlying the color change of the FT-SCLs within freeze-thaw cycling. It has been well known that the PVA solutions undergo a sol-gel transition after repeated freeze-thaw processes rather than the sole freezing or thawing process.[29] Upon exposure to subzero temperatures, the freezing of water drives the phase separation of PVA chains from the solvents, which facilitates the formation of crystalline regions via hydrogen bonding.[30] However, the formation of a mechanically stable hydrogel network still relies on repeated freeze-thaw cycles, where the thawing process is important for expanding the free volume of PVA chains for additional crystallization in the following freezing processes, thereby generating physically cross-linked networks.[29] Therefore, the PVA chains within the FT-SCLs will gradually form physically cross-linked networks with the increased numbers of freeze-thaw cycles (**Figure 3**A), which will affect the inter-particle distance of the PS particles within the PVA matrix and the refractive index – two key factors determining the structural color of the FT-SCLs according to the following Bragg-Snell equation:

$$\lambda_{max} = 1.633\frac{d}{m}\sqrt{\sum n_i^2 V_i - \sin^2\theta} \quad (1)$$

where λ_{max} is the wavelength of reflectance peak, d is the inter-particle distance of colloidal particles, m is the diffraction order, n_i and ϕ_i are the refractive index and volume fraction of colloidal arrays suspension, and θ is the angle between the sample normal and incident light.

Consistent with the above theoretical analyses, the crystallization of PVA under freeze-thaw cycles can be verified by small-angle X-ray scattering (SAXS), as indicated by increased sizes of scattering ring and decreased scatter factor q (Figure 3B,C). The enhancement of the crystallization can further be validated by X-ray diffraction (XRD), where the intensity of the characteristic PVA crystalline peaks of 20.8° (corresponding to the (101) lattice plane) slightly increases with the increase of freeze-thaw cycle number (Figure 3D). Moreover, the sol-gel transition can be confirmed by rheological measurements, as indicated by the higher storage modulus (G′) than the loss modulus (G″) when the temperature is below −1.6 °C (Figure 3E), corresponding to the initiation of the sol-gel transition.[31] These results reveal the definitive correlation between the crystallization-induced physical cross-linking and the sol-gel transition of the FT-SCLs under freeze-thaw cycling, subsequently resulting in shrinking networks that compress the periodic structures of colloid particles within them, as evidenced by decreased inter-particle distances (from 267 to 230 nm) and increased refractive index (from 1.467 to 1.498) upon exposure to 3 freeze-thaw cycles (Figure 3F; Figure S10, Supporting Information). Collectively, the irreversible sol-gel transition and the accompanying shrinkage of periodic structures under freeze-thaw cycling endow the FT-SCLs with unique colorimetric freeze-thaw monitoring capabilities. However, it is impossible for the PVA-free samples, which only undergo reversible phase transitions and show unchanged color when exposed to the same repeated freeze-thaw processes (Figure S11, Supporting Information).

2.4. Applications of FT-SCLs

Leveraging their unique capabilities in irreversibly altering colors under repeated freeze-thaw processes, the FT-SCLs have been used as intelligent labels for vaccine storage and whole blood preservation. For the vaccines that shall not be exposed for more than 1 freeze-thaw cycle,[1] we choose the PA_{10}-FT-SCLs as intelligent labels, which are simply pasted on the vaccine vial (**Figure 4**A). Once the vaccines undergo risky 2 freeze-thaw cycles, the PA_{10}-FT-SCLs will show naked-eye recognizable color changes from red to green (Figure 4A), where the shift of reflection peak exceeds 36 nm (Figure 4B). The FT-SCLs-based intelligent labels provide a facile method for alerting the freeze-thaw damage of vaccines, with superior convenience over the traditional shake tests. The whole blood is another representative bio-product whose potency is highly susceptible to freeze-thaw cycling.[32] To alert the freeze-thaw damage, we pasted an intelligent label consisting of FT-SCLs and a colorimetric card onto a blood bag (Figure 4C). After 1st, 2nd, and 3rd freeze-thaw cycles,

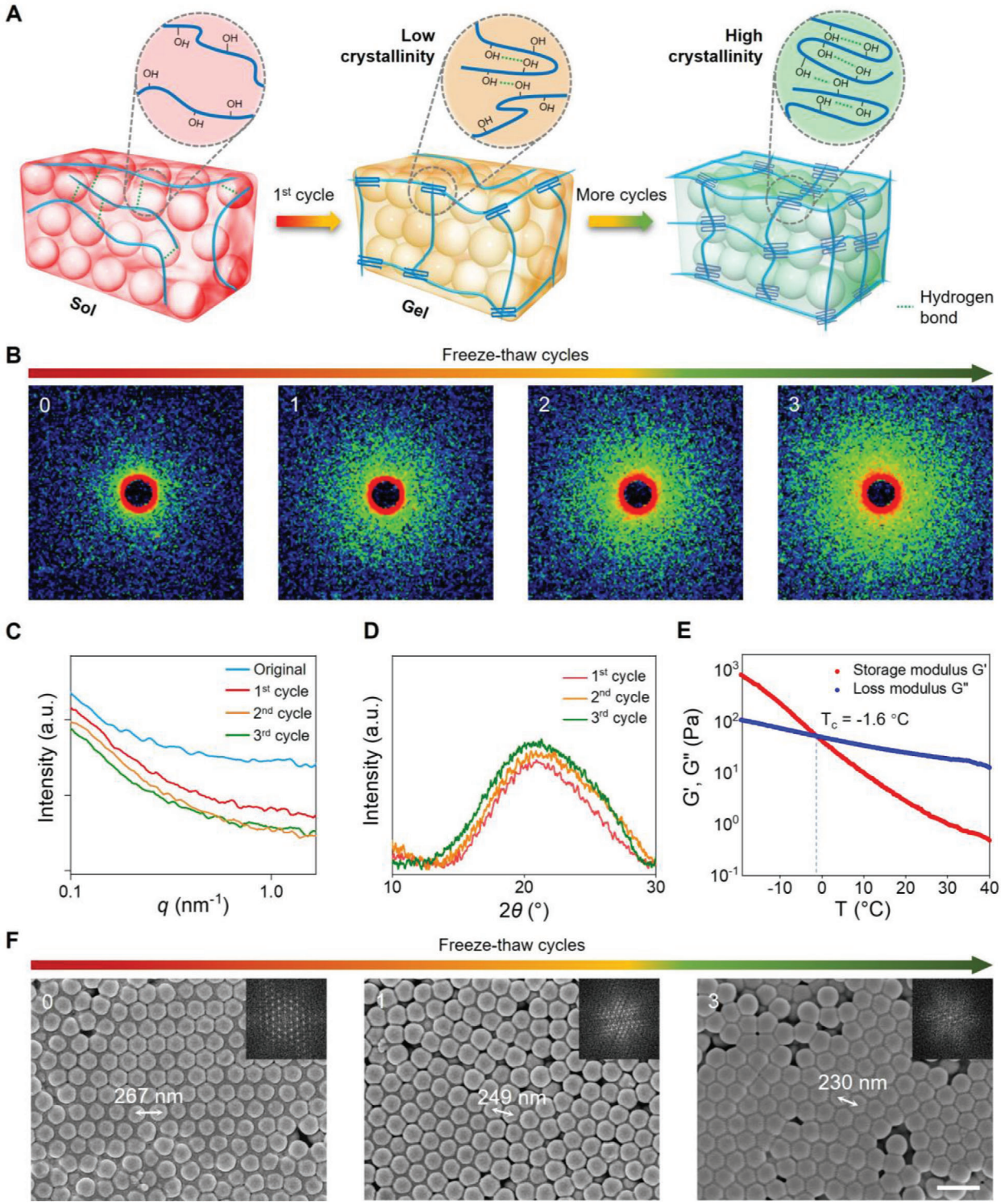

Figure 3. Freeze-thaw monitoring mechanisms. A) Schematic illustration of changed arrangements of colloidal particles induced by sol-gel transition under multiple freeze-thaw cycles. The multiple freeze-thaw processes lead to increased crystallization of PVA that generates physically cross-linked networks, resulting in a decreased lattice distance of the assembled colloidal particles. B- The SAXS spectra (B), SAXS patterns (C), and XRD patterns (D) of samples under 0–3 freeze-thaw cycles with the freezing temperature of −20 °C and the thawing temperature of 8 °C. E) Temperature dependence of storage modulus (G') and loss modulus (G") for PVA solutions formulated by using PVA with 88% alcoholysis degree at an angular frequency of 6.28 rads s^{-1} and a cooling rate of 3 °C min^{-1}. F) SEM and fast Fourier transformation (FFT) images show varying inter-particle distances of the FT-SCLs under multiple freeze-thaw cycles: the original state (*d*: 267 nm), the state after the 1st freeze-thaw cycle (*d*: 249 nm), and the state after 3rd freeze-thaw cycle (*d*: 230 nm). Scale bars: 500 nm.

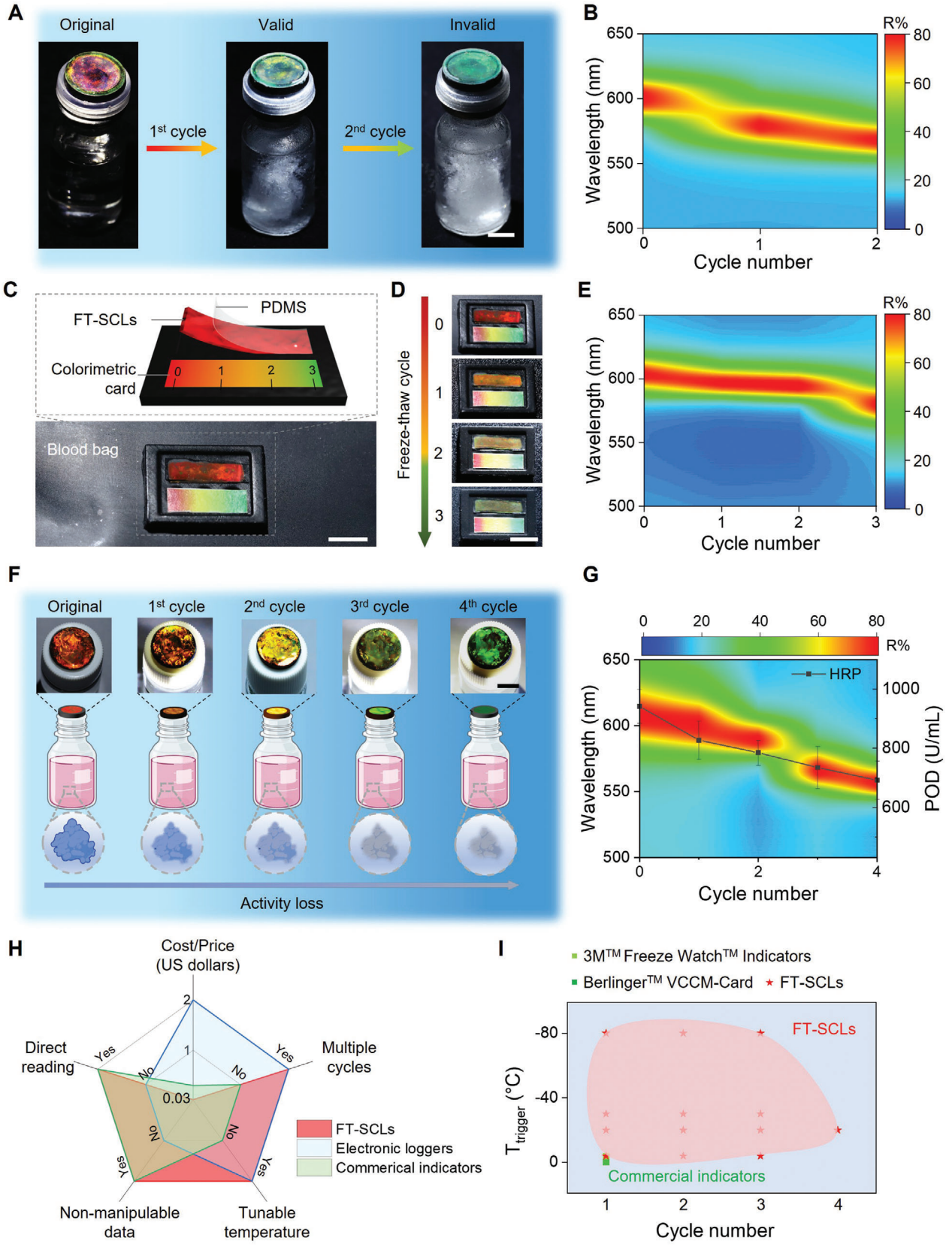

the color of the FT-SCLs in the label turns red, yellow, and green (Figure 4D), with shifts of reflection peak to 600, 586, and 570 nm, respectively (Figure 4E). With the assistance of the accompanying colorimetric card, the exact number of freeze-thaw cycles can be facilely documented in a colorimetric manner, showing the promise of quality control for bio-products during cold-chain storage or transport.

Beyond visualized monitoring the freeze-thaw damage of bio-products, the FT-SCLs can further be used for tracking enzyme stability under freeze-thaw cycling in a lossless and colorimetric manner, which conventionally depends on expensive test kits and complex instruments.[33] We employed horseradish peroxidase (HRP) as a model enzyme, which has been broadly used in biosensing and bioremediation.[34], and the PA_5-FT-SCLs as the intelligent labels (Figure 4C). By synchronously tracking the bioactivity of the HRP and the color of the labels, we observe that the color of the labels turns orange, yellow, olive, and green after 1 to 4 freeze-thaw cycles (Figure 4F), where the bioactivity of HRP correspondingly loses 12, 17, 22, and 27%, respectively, as indicated by the test kit for peroxidase (POD, Figure 4G). Remarkably, the decreased reflection peak of the PA_5-FT-SCLs (from originally 605 to 601, 589, 567, and ultimately 556 nm) fits well with the declined bioactivity of HRP with the increase of freeze-thaw cycle number (Figure 4D), providing an alternative method to monitor the bioactivity loss of enzymes during repeated freeze-thaw processes.

In comparison with the high price of traditional electronic loggers (≈2 dollars each item) and existing commercial intelligent labels (i.e., Berlinger VCCM-Card and 3 M Freeze Watch Indicators, ≈0.3 dollars each item), the estimated cost of the FT-SCLs-based intelligent labels will be quite low (≈0.03 dollars each item) excluding pricing factors related to the practical production process (Figure 4H). Furthermore, the FT-SCLs circumvent the shortages of traditional electronic loggers, including manipulable data and inconvenient readout, as well as the problems of existing commercial intelligent labels that cannot monitor the freeze-thaw processes with multiple cycles and/or diverse triggered temperatures (Figure 4H). Overall, the FT-SCLs-based intelligent labels will exhibit superior adaptability and versatility in practical applications thanks to their adjustable sensitivity across practically relevant temperature ranges (−80–−4 °C) and customizable response thresholds (Figure 4I)

3. Conclusion

In summary, we develop a kind of FT-SCLs that can track the freeze-thaw history in a visualized manner by harnessing their irreversible sol-gel phase transition under freeze-thaw cycling. The FT-SCLs show excellent color stability in the common conditions of cold-chain storage or transport (0, 8, or −20 °C) over dozens of days. Upon exposure to repeated freeze-thaw cycles, the FT-SCLs undergo irreversible sol-gel transition and unidirectional alteration of their periodic structures, therefore imparting stepwise and unrecoverable color change (from red to green) to indicate the exact number of freeze-thaw cycles. By modulating the sol-gel transition, the FT-SCLs demonstrate adjustable sensitivity across practically relevant temperature ranges (−80–−4 °C) and customizable response thresholds. Such FT-SCLs can be used for not only the vaccines requiring highly sensitive color alteration within one freeze-thaw cycle but also the identification of enzyme bioactivity loss by recording multiple cycles, which further hold great promise in the fields of cell cryopreservation and the food industry.

4. Experimental Section

Materials: Styrene (99%), acrylic acid (99%), ammonium persulfate (99%), glycerol (99%), and Dulbecco's phosphate buffered saline (DPBS) were purchased from Sigma-Aldrich (USA). Polyvinyl alcohol (alcoholysis degree: 80%, 88%, M_w≈78 000) and phytic acid solution (50 wt% in water) were purchased from Aladdin Biochemical Technology (Shanghai, China). Polydimethylsiloxane (PDMS, Sylgard 184 silicone elastomer kit) was purchased from Dow Corning Co., Ltd. (Midland, USA). Multiple-wall carbon nanotubes (MWCNTs, average length: 20 μm), and carbon black powder were purchased from Xianfeng Nano Co., Ltd. (Nanjing, China). Peroxidase from horseradish (300 units mg^{-1}) and Congo red were purchased from Shanghai Macklin Biochemical Co. Ltd. (Shanghai, China). Ultrapure water (18.2 MΩ·cm) was produced by a water purification system (Arioso Power II, Human, Korea) and used throughout this study.

Fabrication of FT-SCLs: To fabricate the FT-SCLs, colloidal monodispersed PS colloidal particles were first synthesized through soap-free emulsion polymerization according to the previous studies.[21a] In a typical experiment, 17.5 g styrene and 0.95 g acrylic acid were dissolved in 100 mL ultra-pure water to formulate a solution in a 250 mL flask. After heating the solution at 110 °C for 10 min, a 5 mL 3.5 w $v\%^{-1}$ ammonium persulfate aqueous solution was added under mechanical stirring at 300 rpm, followed by continuous reflux at 110 °C for 3 h to form the PS colloidal particles. The as-synthesized PS colloidal particles were purified by centrifuge and washed with water at least 3 times. The PS colloidal particles with different diameters were fabricated by adding different amounts of acrylic acid from 0.95 to 1.15 g. Then, a PVA solution was prepared by dissolving PVA (alcoholysis degree: 80% or 88%) in a DMSO/water (50/50/w) mixture solvent at 85 °C under vigorous stirring for 2 h. The PVA solution was subsequently mixed with glycerol and carbon black in a mass ratio of 90.0:9.8:0.2 to formulate a suspension after degassing by ultrasonication for 10 min. The PS colloidal particles were dispersed within the suspension at different mass ratios (30, 40, 50, or 60 wt%). After sufficient stirring and degassing for 24 h, the FT-SCLs were formed through spontaneous assembly of the PS particles within the suspension. The FT-SCLs

Figure 4. Applications of FT-SCLs. A) Schematic illustration and macroscopic images of the PA_{10}-FT-SCLs for indicating the freeze-thaw history of a vaccine. Scale bar: 5 mm. B) The dynamic reflectance contour spectra of the PA_{10}-FT-SCLs intelligent labels for monitoring the vaccines within 2 freeze-thaw cycles with the freezing temperature of −20 °C and thawing temperature of 8 °C. C) The schematic diagram and macroscopic images of the label for colorimetric monitoring the freeze-thaw exposure of whole blood. Scale bar: 1 cm. D,E) Macroscopic images (D) and dynamic reflectance contour spectra (E) of the label pasted on a blood bag under multiple freeze-thaw cycles with the freezing temperature of −20 °C and thawing temperature of 8 °C. Scale bar: 1 cm. F) Schematic diagram and macroscopic images of the FT-SCLs for indicating the declined bioactivities of HRP under repeated freeze-thaw cycles. Scale bar: 1 cm. G) The bioactivity of HRP enzyme and dynamic reflectance contour spectra of the PA_5-FT-SCLs labels within 4 freeze-thaw cycles with the freezing temperature of −20 °C and thawing temperature of 8 °C. H) Comparison among FT-SCLs, traditional temperature-time electronic loggers, and commercial intelligent labels in terms of cost/price, readout modes, data processing, triggered temperature, and the number of freeze-thaw cycles allowed in the monitoring. I) Comparison between FT-SCLs labels and commercial intelligent labels in applicable ranges of freeze-thawing monitoring.

were also processed into labels with the assistance of different types of pre-shaped black PDMS molds (QR-code molds: length × width × height = 15 mm × 15 mm × 2 mm, length × width × depth = 0.8 mm × 0.8 mm × 0.05 mm for each pixel; round molds: diameter × depth = 13 mm × 0.05 mm) that contain 1 wt% MWCNTs.

Evaluation of FT-SCLs in Freeze-Thaw Monitoring: To investigate the color stability of FT-SCLs in either freezing or thawing conditions, the FT-SCLs labels were placed at −20 °C for 14 days, otherwise 0 or 8 °C for 28 days, and the colors within this period were recorded by a bright-field optical microscope (SZ 69, Olympus, Japan). The reflection was characterized by a fiber-optic spectrometer (HR 2000+, Ocean Optics, USA). To examine the freeze-thaw monitoring performance of the FT-SCLs, different types of FT-SCLs labels were prepared, which include the rounded FT-SCLs labels prepared as mentioned above, the FT-SCLs prepared by using the PVA with 80% alcoholysis degree, or the PA-added FT-SCLs that contain different contents of PA (5, 10, and 20 wt%). In typical experiments, the samples were frozen at a specific freezing temperature (−20, −80, −30, or −4 °C) for 2 h and then thawed at 8 °C for 1 h. The colors and reflection spectra of the samples after different freeze-thaw cycles were recorded by the microscope and the fiber-optic spectrometer. Additionally, we also prepared the PVA-free samples using a 50 v v%$^{-1}$ DMSO-water mixture solvent, whose colors and reflection spectra under similar multiple freeze-thaw cycles with a freezing temperature of −20 °C and a thawing temperature of 8 °C were also recorded.

In proof-of-concept studies, we prepared PA_{10}-FT-SCLs labels and pasted them onto vaccine vials. Which then underwent repeated freeze-thaw processes (−20 °C for 2 h and 8 °C for 1 h). The colors and reflection spectra of the FT-SCLs after three freeze-thaw cycles were recorded. Besides, we also pasted PA_5-FT-SCLs labels on the bottles that contained HRP suspensions (0.2 U mL^{-1}). The colors and reflection spectra of the PA_5-FT-SCLs labels within 4 freeze-thaw cycles were tracked. The bioactivities of HRP within the multiple freeze-thaw cycles were also characterized by using the test kit of POS (Beijing Solarbio Science, China) according to the manufacturer's protocol. Moreover, we further prepared FT-SCLs labels and pasted them onto blood bags, where a Congo red aqueous solution (0.15 wt%) was packaged for simulating blood. The colors and reflection spectra of the FT-SCLs on the blood bags were also measured within 3 freeze-thaw cycles.

Characterizations: The macroscopic photos of the FT-SCLs samples were taken by a digital camera (Canon, EOS 6D Mark II, Japan). The microscopic optical images were captured by a bright-field optical microscope. The in situ reflection spectra were measured by a fiber-optic spectrometer, which was coupled with an optical microscope (Ni-U, Nikon, Japan). The microstructures of the FT-SCLs samples were characterized by a field-emission scanning electron microscope (FE-SEM, Sigma 300, Zeiss, Germany). The rheological behavior of the PVA hydrogel was characterized by rheological testing (Mars 60, Haake, Germany), where the temperature sweep was measured from −30 to 30 °C (3 °C min^{-1}) at a fixed frequency of 6.28 rads s^{-1}. The crystallization of samples was characterized by both wide-angle X-ray diffraction (XRD, D8 Venture, Bruker, Germany) using Cu Kα radiation (λ = 0.154 nm) in the 2θ range of 10°–65° with a scan rate of 2° min^{-1} and small-angle X-ray scattering (SAXS, Xeuss 2.0, Xenocas, France) using a Cu point-focused source at 40 kV. The scattering vector is defined as $q = 4\pi / \lambda \sin\theta$, where λ is the wavelength of the X-ray beam (λ = 0.154 nm) and 2θ is the scattering angle. The refractive index was characterized by an ellipsometer (IR-Vase Mark II M-2000UI, J.A. Woolam, USA).

Supporting Information

Supporting Information is available from the Wiley Online Library or from the author.

Acknowledgements

The authors acknowledge the financial support provided by the Shenzhen Medical Research Fund (B2302045), the National Natural Science Foundation of China (52261160380, 52303289), the Youth Innovation Promotion Association of CAS (Y2023100), and the Fundamental Research Program of Shenzhen (RCJC20221008092729033, JCYJ20220818101800001).

Conflict of Interest

The authors declare no conflict of interest.

Author Contributions

X.D. conceived the idea and supervised the study. Q.Z. and C.H. conducted the experiments, analyzed the results, and wrote the manuscript. X.D. revised the manuscript. All authors contributed to the discussion and interpretation of the results.

Data Availability Statement

The data that support the findings of this study are available in the supplementary material of this article.

Keywords

colorimetric sensor, freezing-thawing monitoring, intelligent label, photonic crystal, structural color liquid

Received: January 9, 2025
Revised: February 20, 2025
Published online:

[1] World Health Organization, https://pesquisa.bvsalud.org/portal/resource/pt/who-311278 (accessed: July **2019**).
[2] a) S. C. Arya, *Vaccine* **2000**, *19*, 595; b) J. Smith, M. Lipsitch, J. W. Almond, *Lancet* **2011**, *378*, 428.
[3] D. M. Matthias, J. Robertson, M. M. Garrison, S. Newland, C. Nelson, *Vaccine* **2007**, *25*, 3980.
[4] T. Wirkas, S. Toikilik, N. Miller, C. Morgan, C. J. Clements, *Vaccine* **2007**, *25*, 691.
[5] a) H. Tao, M. A. Brenckle, M. M. Yang, J. D. Zhang, M. K. Liu, S. M. Siebert, R. D. Averitt, M. S. Mannoor, M. C. McAlpine, J. A. Rogers, D. L. Kaplan, F. G. Omenetto, *Adv. Mater.* **2012**, *24*, 1067; b) U. Kartoglu, N. K. Ozguler, L. J. Wolfson, W. Kurzatkowski, *Bull World Health Organ.* **2010**, *88*, 624.
[6] a) D. X. Chen, A. Tyagi, J. Carpenter, S. Perkins, D. Sylvester, M. Guy, D. D. Kristensen, L. J. Braun, *Hum. Vaccines* **2009**, *5*, 26; b) A. Arsiccio, R. Pisano, *J. Pharm. Sci.* **2020**, *109*, 2116; c) E. H. Cao, Y. H. Chen, Z. F. Cui, P. R. Foster, *Biotechnol. Bioeng.* **2003**, *82*, 684.
[7] O. S. Kumru, S. B. Joshi, D. E. Smith, C. R. Middaugh, T. Prusik, D. B. Volkin, *Biologicals* **2014**, *42*, 237.
[8] S. D. Wang, X. H. Liu, M. Yang, Y. Zhang, K. Y. Xiang, R. Tang, *Packag. Technol. Sci.* **2015**, *28*, 839.
[9] a) J. R. Allegra, R. H. Baughman, *Vaccine* **2020**, *38*, 6967; b) S. Choi, Y. Eom, S. M. Kim, D. W. Jeong, J. Han, J. M. Koo, S. Y. Hwang, J. Park, D. X. Oh, *Adv. Mater.* **2020**, *32*, 1907064; c) L. T. Hao, M. Lee, H. Jeon, J. M. Koo, S. Y. Hwang, D. X. Oh, J. Park, *ACS Omega* **2021**, *6*, 8598; d) L. Romano, A. Portone, M. B. Coltelli, F. Patti, R. Saija, M. A. Iati, G. Gallone, A. Lazzeri, S. Danti, O. M. Marago, A. Camposeo, D. Pisignano, L. Persano, *Nat. Commun.* **2020**, *11*, 5991; e) H. Yousefi, M. M. Ali, H. M. Su, C. D. M. Filipe, T. F. Didar, *ACS Nano* **2018**, *12*, 3287.

[10] M. Weston, S. Geng, R. Chandrawati, *Adv. Mater. Technol.* **2021**, *6*, 2001242.
[11] a) C. Zhang, A. X. Yin, R. B. Jiang, J. Rong, L. Dong, T. Zhao, L. D. Sun, J. F. Wang, X. Chen, C. H. Yan, *ACS Nano* **2013**, *7*, 4561; b) D. H. Kou, L. Gao, R. C. Lin, S. F. Zhang, W. Ma, *Adv. Sci.* **2024**, *11*, 2310060.
[12] a) M. Nie, C. Huang, X. Du, *Nanoscale* **2021**, *13*, 2780; b) Q. Zhao, Y. Wang, H. Cui, X. Du, *J. Mater. Chem. C* **2019**, *7*, 6493; c) J. Ge, Y. Yin, *Angew. Chem., Int. Ed.* **2011**, *50*, 103089; d) Y. Hu, Z. Tian, D. Ma, C. Qi, D. Yang, S. Huang, *Adv. Colloid Interface Sci.* **2024**, *324*, 103089; e) F. Wang, M. Liu, C. Liu, C. Huang, L. Zhang, A. Cui, Z. Hu, X. Du, *Natl. Sci. Rev.* **2023**, *10*, nwac164.
[13] Y. Shang, C. Huang, Z. Li, X. Du, *Adv. Funct. Mater.* **2025**, *35*, 2412703.
[14] a) A. C. Arsenault, D. P. Puzzo, I. Manners, G. A. Ozin, *Nat. Photonics* **2007**, *1*, 468; b) K. Chen, Q. Q. Fu, S. Y. Ye, J. P. Ge, *Adv. Funct. Mater.* **2017**, *27*, 1702825.
[15] a) Z. W. Li, C. Qian, W. J. Xu, C. H. Zhu, Y. D. Yin, *Sci. Adv.* **2021**, *7*, eabh1289; b) L. He, M. S. Wang, J. P. Ge, Y. D. Yin, *Acc. Chem. Res.* **2012**, *45*, 1431; c) M. S. Wang, Y. D. Yin, *J. Am. Chem. Soc.* **2016**, *138*, 6315.
[16] a) Y. Wang, Q. Zhao, X. Du, *J. Mater. Chem. B* **2020**, *8*, 3519; b) Y. Wang, H. Cui, Q. Zhao, X. Du, *Matter* **2019**, *1*, 626; c) X. Du, S. H.-M. Chiu, D. H.-C. Ong, R. Vellaisamy, M. H.-W. Lam, *Sens. Actuators, B* **2016**, *223*, 318; d) X. Du, N. Y. Lei, P. Hu, Z. Lei, D. H. Ong, X. Ge, Z. Zhang, M. H. Lam, *Anal. Chim. Acta* **2013**, *787*, 193; e) X. Du, N.-Y. Lei, H.-M. Chiu, X. Ge, Z. Zhang, M. Hon-Wah Lam, *J. Mater. Chem. B* **2013**, *1*, 1535.
[17] a) J. W. Kim, Y. Oh, S. Lee, S. H. Kim, *Adv. Funct. Mater.* **2021**, *32*, 2107275; b) Y. Wang, Q. Zhao, X. Du, *Mater. Horiz.* **2020**, *7*, 1341; c) X. Du, H. Cui, T. Xu, C. Huang, Y. Wang, Q. Zhao, Y. Xu, X. Wu, *Adv. Funct. Mater.* **2020**, *30*, 1909202; d) Z. Hu, X. Lu, J. Gao, *Adv. Mater.* **2001**, *13*, 1708; e) J. H. Kang, J. H. Moon, S. K. Lee, S. G. Park, S. G. Jang, S. Yang, S. M. Yang, *Adv. Mater.* **2008**, *20*, 3061; f) J. D. Debord, L. A. Lyon, *J. Phys. Chem. B* **2000**, *104*, 6327; g) S. Y. Lee, J. S. Lee, S. H. Kim, *Adv. Mater.* **2019**, *31*, 1901398; h) Y. Wang, Z. Zhang, H. Chen, H. Zhang, H. Zhang, Y. Zhao, *Sci. Bull.* **2022**, *67*, 512; i) Y. Hu, Z. Tian, D. Ma, C. Qi, D. Yang, S. Huang, *Nat. Commun.* **2024**, *15*, 5643.
[18] a) Y. Liu, Q. S. Fan, G. H. Zhu, G. P. Shi, H. R. Ma, W. Li, T. L. Wu, J. T. Chen, Y. D. Yin, J. G. Guan, *Mater. Horiz.* **2021**, *8*, 2032; b) B. T. Zhu, Q. Q. Fu, K. Chen, J. P. Ge, *Angew. Chem. Int. Ed.* **2018**, *57*, 252; c) Q. Q. Fu, H. M. Zhu, J. P. Ge, *Adv. Funct. Mater.* **2018**, *28*, 1804628.
[19] C. Huang, Y. Shang, J. Hua, Y. Yin, X. Du, *ACS Nano* **2023**, *17*, 10269.
[20] a) G. Jia, Y. Chen, A. Sun, V. Orlien, *Compr. Rev. Food Sci. Food Saf.* **2022**, *21*, 2433; b) A. Murray, T. R. Congdon, R. M. F. Tomas, P. Kilbride, M. I. Gibson, *Biomacromolecules* **2022**, *23*, 467.
[21] a) X. Du, T. Li, L. Li, Z. Zhang, T. Wu, *J. Mater. Chem. C* **2015**, *3*, 3542; b) Z.-Z. Gu, H. Chen, S. Zhang, L. Sun, Z. Xie, Y. Ge, *Colloids Surf., A* **2007**, *302*, 312.
[22] Y. Li, Q. Fan, X. Wang, G. Liu, L. Chai, L. Zhou, J. Shao, Y. Yin, *Adv. Funct. Mater.* **2021**, *31*, 2010746.
[23] a) H. Adelnia, R. Ensandoost, S. S. Moonshi, J. N. Gavgani, E. I. Vasafi, H. T. Ta, *Eur. Polym. J.* **2022**, *164*, 110974; b) F. Yokoyama, I. Masada, K. Shimamura, T. Ikawa, K. Monobe, *Colloid Polym. Sci.* **1986**, *264*, 595.
[24] a) X. Wang, Y. Qiu, G. Chen, Z. Chu, A. Shadike, C. Chen, C. Chen, Z. Zhu, *ACS Appl. Polym. Mater.* **2020**, *2*, 2086; b) C. Chen, Y. Zhu, H. Bao, P. Zhao, H. Jiang, L. Peng, X. Yang, C. Li, *Soft Matter* **2011**, *7*, 915; c) M. M. Muscatello, S. A. Asher, *Adv. Funct. Mater.* **2008**, *18*, 1186.
[25] M. N. Uddin, M. A. Roni, *Vaccines* **2021**, *9*, 1033.
[26] S. Chen, H. Yang, K. Huang, X. Ge, H. Yao, J. Tang, J. Ren, S. Ren, Y. Ma, *Polymers* **2021**, *13*, 3778.
[27] R. C. Bortolin, J. Gasparotto, A. R. Vargas, M. D. Morrone, A. Kunzler, B. S. Henkin, P. R. Chaves, S. Roncato, D. P. Gelain, J. C. F. Moreira, *Biopreserv. Biobanking* **2017**, *15*, 182.
[28] S. Zhang, Y. Zhang, B. Li, P. Zhang, L. Kan, G. Wang, H. Wei, X. Zhang, N. Ma, *ACS Appl. Mater. Interfaces* **2019**, *11*, 32441.
[29] C. M. Hassan, N. A. Peppas, *Macromolecules* **2000**, *33*, 2472.
[30] C. W. Bunn, *Nature* **1948**, *161*, 929.
[31] N. Joshi, K. Suman, Y. M. Joshi, *Macromolecules* **2020**, *53*, 3452.
[32] R. C. Bortolin, J. Gasparotto, A. R. Vargas, M.da Silva Morrone, A. Kunzler, B. S. Henkin, P. R. Chaves, S. Roncato, D. P. Gelain, J. C. F. Moreira, *Biopreserv. Biobanking* **2017**, *15*, 182.
[33] a) T. R. Northen, J. C. Lee, L. Hoang, J. Raymond, D. R. Hwang, S. M. Yannone, C. H. Wong, G. Siuzdak, *Biochemistry* **2008**, *105*, 3678; b) M. J. Todd, J. Gomez, *Anal. Biochem.* **2001**, *296*, 179.
[34] K. Sellami, A. Couvert, N. Nasrallah, R. Maachi, M. Abouseoud, A. Amrane, *Sci. Total Environ.* **2022**, *806*, 150500.